Transcription-induced active forces suppress chromatin motion by inducing a transient disorder-to-order transition

Sucheol Shin,[1] Hyun Woo Cho,[2] Guang Shi,[1,3] and D. Thirumalai[1,*]

[1] *Department of Chemistry, The University of Texas at Austin, Texas 78712, USA*
[2] *Department of Fine Chemistry and Center for Functional Biomaterials, Seoul National University of Science and Technology, Seoul 01811, Republic of Korea*
[3] *Department of Materials Science, University of Illinois, Urbana, Illinois 61801, USA*

(Dated: September 15, 2022)

Recent experiments have shown that the mobility of human interphase chromosome decreases during transcription, and increases upon inhibiting transcription, a finding that is counter-intuitive because it is thought that the active mechanical force (F) generated by RNA polymerase II (RNAPII) on chromatin would render it more open and mobile. Inspired by these observations, we use a copolymer model to investigate how F affects the dynamical properties of a single chromatin. The movements of the loci in the gene-rich region are suppressed in an intermediate range of F, and are enhanced at small and large F values. In the intermediate F, the bond length between consecutive loci increases, becoming commensurate with the location of the minimum in the attractive interaction between the active loci. This results in a transient disorder-to-order transition, leading to the decreased mobility during transcription. Transient ordering of the loci in the gene-rich region might be a mechanism for nucleating a dynamic network involving transcription factors, RNAPII, and chromatin.

Advances in experimental techniques [1, 2] have elucidated the organizational details of chromosomes, thus deepening our understandings of how gene regulation is connected to chromatin structure [3]. Relatively less is known about the dynamics of the densely packed interphase chromosomes in the cell nucleus. Experimental and theoretical studies have shown that the locus dynamics is heterogeneous, exhibiting sub-diffusive behavior [4–7], which is consistent with models that [8–10] predict glass-like dynamics. However, it is challenging to understand the dynamic nature of chromosomes that governs the complex subnuclear processes, such as gene transcription.

The link between transcriptional activity and changes in chromosomal dynamics is important in understanding the dynamics of chromosomes in distinct cell types and states [11, 12]. It is reasonable to expect that transcription of the active gene-rich region could make it more expanded and dynamic [13, 14]. However, active RNA polymerase (RNAP) II suppressed the movement of the nucleosomes [12]. Let us first summarize the key experimental results, which inspired our study: (1) By imaging the motion of individual nucleosomes in live human cells, it was shown that the mean square displacements (MSDs) of the nucleosomes during active transcription are constrained (Fig. S1 [15]). (2) When the cells were treated with α-amanitin (α-AM) or DRB, which selectively block the translocation of RNAPII [16, 17], the mobility of the nucleosomes was enhanced. This finding is counter-intuitive because the elongation process generates mechanical forces [18, 19] that could render the chromatin more dynamic. (3) The enhanced motion was restricted only to euchromatin loci that are predominantly localized in the cell interior whereas the dynamics of heterochromatin, found in the periphery, is unaffected by transcription. Based on these observations, it was hypothesized that RNAPs and other protein complexes, facilitating transcription, transiently stabilize chromatin by forming dynamic clusters [20–23]. This hypothesis is challenged, however, because inhibition by DRB mainly leads to stalling of RNAPs bound to chromatin [17]. Moreover, transcriptional inhibition does not significantly alter the higher-order structures of chromosomes [23, 24]. These observations raise the question: Is there a physical explanation for the increased chromatin dynamics upon inhibition of transcription and a decrease during transcription? We provide a plausible answer to this question using a simple model.

Using the experimental results as a backdrop, we theorize that RNAPII exerts active force [18, 19] in a vectorial manner on the active loci. We then examine the effects of active force on the organization and dynamics of chromosome using the Chromosome Copolymer Model (CCM) [9]. The CCM faithfully captures the Hi-C experimental results, showing microphase separation between euchromatin (A-type loci) and heterochromatin (B-type loci) on large length scale and formation of topologically associating domains (TADs) on a smaller length scale in interphase chromosomes. The CCM chain, like interphase chromosomes, is condensed, exhibiting glass-like dynamics in the absence of activity, in agreement with experiments [4, 9]. We perform Brownian dynamics simulations of a single chromosome with active force. Our key results are: (i) In accord with experiments [12], the dynamics of the active loci, measured using the MSD, is suppressed upon application of the active force. Despite the simplification, our simulations qualitatively capture the relative increase in the MSD for the transcriptionally inactive case. (ii) The decrease in the A loci's mobility

occurs over a specific range of activity level. Surprisingly, in this range the segregated A-loci undergo a transient disorder-to-order transition, resembling a face-centered cubic (FCC) lattice, whereas the B loci remain fluid-like. (iii) Chromosome in which the epigenetic sequence is random cannot capture the experimental observations.

We model an interphase chromosome as a flexible self-avoiding copolymer (Fig. 1) [15]. Interactions between non-adjacent pairs of loci are modeled by the Lennard-Jones (LJ) potential. The relative strengths of interactions between the loci is constrained by the Flory-Huggins theory [25, 26], which ensures microphase separation between the A and B loci. Specific locus pairs are anchored to each other, representing the chromatin loops mediated by CTCFs [27]. In this study, a 4.8-Mbp segment of human chromosome 5 is coarse-grained using $N = 4{,}000$ loci (1.2 kbp per locus). The A- to B-type ratio is $N_{\rm A}/N_{\rm B} = 982/3018 \approx 1/3$ [15].

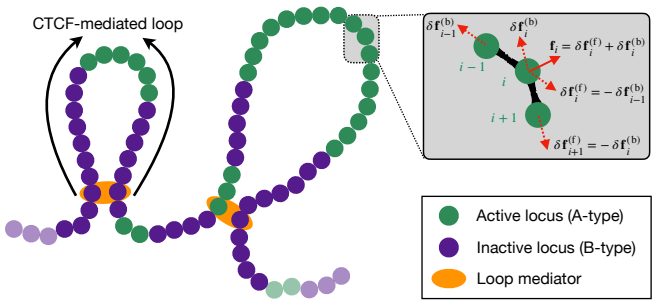

FIG. 1. Schematic depiction of the CCM. Chromosome is modeled as a copolymer chain consisting of active/inactive (green/purple-colored) loci. Specific locus pairs are connected by loop mediators (orange color). The gray box illustrates how active forces are imposed on $i^{\rm th}$ locus and its bonded loci. We apply active forces only to the gene-rich A-type loci.

We applied active forces on the chain to mimic force generated during transcription. Previous theoretical studies [28–31] have considered different forms of active forces on homopolymers and melts of polymer rings. Potential connection to chromatin in the presence of active forces, modeled in an entirely different manner, has also been attempted [32]. We model the active force acting along each bond vector of the A-type loci in an extensile manner, ensuring momentum conservation (dotted arrows in the gray box of Fig. 1). The force, associated with the translocation of RNAP and the nucleosome sliding [18, 19], results in volume exclusion between the bonded A loci (Fig. S2). For the bond vector, $\mathbf{b}_i = \mathbf{r}_{i+1} - \mathbf{r}_i$, force, $\delta\mathbf{f}^{(\rm f)}_{i+1} = f_0\hat{\mathbf{b}}_i$, is exerted on $(i+1)^{\rm th}$ locus in the forward direction, where f_0 is the force magnitude and $\hat{\mathbf{b}}_i = \mathbf{b}_i/|\mathbf{b}_i|$, and $\delta\mathbf{f}^{(\rm b)}_i = -\delta\mathbf{f}^{(\rm f)}_{i+1}$ is exerted on $i^{\rm th}$ locus in the backward direction. We use the dimensionless parameter, $F \equiv f_0\sigma/k_BT$, as a measure of the force magnitude, where σ is the diameter of a single locus, k_B is the Boltzmann constant, and T is the temperature.

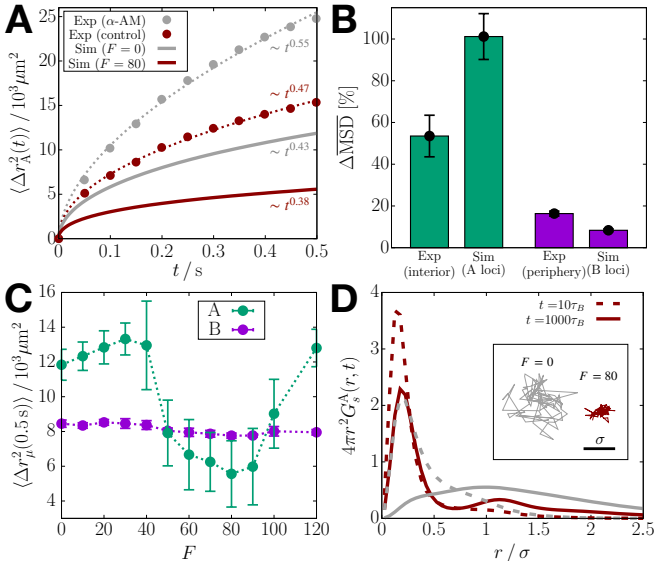

FIG. 2. Transcription-induced active forces reduce the euchromatin mobility. (A) $\langle\Delta r^2_{\rm A}(t)\rangle$ from simulations with $F = 0$ and $F = 80$ (solid lines), compared with the euchromatin MSD from the experiment that inhibits transcription using α-AM [12] (circles). The dotted lines are the fits to the experimental data. (B) Bar graphs comparing the increase in $\langle\Delta r^2_{\rm A}(t)\rangle$ ($\langle\Delta r^2_{\rm B}(t)\rangle$) shown in panel A (Fig. S3A) between experiment and simulation results. (C) MSDs for the A and B loci at $t = 0.5$ s as a function of F. The dotted lines are a guide to the eye. (D) Radial distributions of the A-locus displacement at $t = 10\tau_B$ (dashed) and $t = 1{,}000\tau_B$ (solid), compared between $F = 0$ (gray) and $F = 80$ (dark-red). The inset shows the 2-D projection of the trajectory of an active locus for $10^4\tau_B$ at $F = 0$ and $F = 80$.

We calculated the MSDs separately for euchromatin and heterochromatin loci, $\langle\Delta r^2_\mu(t)\rangle = \frac{1}{N_\mu}\left\langle\sum_{i=1}^N \delta_{\nu(i)\mu}|\mathbf{r}_i(t) - \mathbf{r}_i(0)|^2\right\rangle$, where $\delta_{\nu(i)\mu}$ is the Kronecker delta (μ =A or B), and $\langle\cdots\rangle$ is the ensemble average. Fig. 2A shows that $\langle\Delta r^2_{\rm A}(t)\rangle$ is smaller at $F = 80$ compared to $F = 0$. This result is comparable to the nucleosome MSDs measured from the interior section of the cell nucleus treated with the transcription inhibitor α-AM [12]. Our simulations capture the change in the scaling exponent, α, extracted from $\langle\Delta r^2_\mu(t)\rangle \sim t^\alpha$ [$\Delta\alpha$(active $\rightarrow$ passive) $= 0.05$ versus 0.08]. However, the magnitude of $\langle\Delta r^2_{\rm A}(t)\rangle$ is smaller in simulations than in experiment. $\langle\Delta r^2_{\rm B}(t)\rangle$ at $F = 80$ is also smaller than at $F = 0$, but the difference is marginal compared to $\langle\Delta r^2_{\rm A}(t)\rangle$, which is consistent with the experimental results for the nuclear periphery (Fig. S3A). We could have obtained better agreement with experiments by tweaking the parameters in the model, which we think is not necessary for the purposes of this study.

In Fig. 2B, we compare the transcription inhibited increase ($\Delta\overline{\rm MSD}$) in the MSD, between experiment and simulations (see Eqs. (S7)-(S8) [15]). We use $F = 80$, which has the smallest MSD (see Fig. 2C), as the control.

The value of f_0 for $F = 80$ is in the range, $f_0 \approx$ 3-16 pN [15], which accords well with forces exerted by RNAP [18]. Comparison between $\Delta\overline{\text{MSD}}$ for the A loci (simulation) and the interior measurements (experiment) is less precise than between the B loci and the periphery. The difference may arise because the interior measurements could include the heterochromatin contribution to some extent, whereas the periphery measurements exclude the euchromatin. Nevertheless, $\Delta\overline{\text{MSD}}$ for all the loci is in better agreement with experiment (Fig. S3C). The reasonable agreement between simulations and experiment is surprising because it is obtained *without adjusting any parameter to fit the data*. Although comparisons in Fig. 2B are made with $F = 80$, we obtain qualitatively similar results for F in the range, $60 \leq F \leq 90$ (Fig. S4).

The simulated MSD, at a given time, changes non-monotonically as F changes. Remarkably, the change is confined to the A loci (Figs. 2C and S3D-S3E); $\langle \Delta r_{\text{A}}^2(0.5\,\text{s})\rangle$ increases modestly as F increases from zero to $F \lesssim 30$, and decreases when F exceeds thirty. There is an abrupt reduction at $F \approx 50$. In the range, $50 \lesssim F \lesssim 80$, $\langle \Delta r_{\text{A}}^2(0.5\,\text{s})\rangle$ continues to decrease before an increase at higher F values. We also calculated the van Hove function, $G_s^{\mu}(\mathbf{r},t) = \left\langle \sum_{i=1}^{N} \delta_{\nu(i)\mu}\delta(\mathbf{r}+\mathbf{r}_i(0)-\mathbf{r}_i(t))\right\rangle / N_{\mu}$, at $t = 10\tau_B \approx 0.007\,\text{s}$ and $1,000\tau_B \approx 0.7\,\text{s}$ [33]. The A-type loci at $F = 80$ do not diffuse as much at $F = 0$ (Fig. 2D), and their displacements are largely within the length scale of σ. In contrast, there is no significant difference in $G_s^{\text{B}}(r,t)$ between $F = 0$ and $F = 80$ (Fig. S3F). Notably, the second peak of $G_s^{\text{A}}(r,t)$ at $F = 80$ hints at the solid-like lattice [34].

To probe the extent to which glass-like behavior [5, 8, 9] is preserved in the presence of RNAPII-induced active forces, we calculated the self-intermediate scattering function, $F_s(k,t) = \frac{1}{N}\sum_{j=1}^{N} e^{i\mathbf{k}\cdot[\mathbf{r}_j(t)-\mathbf{r}_j(0)]}$, where $\mathbf{k}$ is the wave vector. We computed $\langle F_s(k_{\max},t)\rangle$ with $k_{\max} = 2\pi/\sigma$, whose decay indicates the structural relaxation. Time-dependent variations in $\langle F_s(k_{\max},t)\rangle$ (Fig. S5A) show stretched exponential behavior ($e^{-(t/\tau_a)^{\beta}}$; $\beta < 1/3$ at all F values), which is one signature of glass-like dynamics. The decay is even slower if F is increased. The relaxation time, τ_α, calculated using $\langle F_s(k_{\max},\tau_\alpha)\rangle = 0.2$, shows that the relaxation is slowest at $F \approx 80$ (Fig. S5B), which occurs after the dynamical transition in $\langle \Delta r_{\text{A}}^2(0.5\,\text{s})\rangle$ at $F \approx 50$ and before $\langle \Delta r_{\text{A}}^2(0.5\,\text{s})\rangle$ increases beyond $F = 100$ (Fig. 2C). Similarly, when the tails of $\langle F_s(k_{\max},t)\rangle$ were fit with $e^{-(t/\tau_a)^{\beta}}$, the exponent β also exhibits the analogous trend (Fig. S5B). As τ_α increases, β decreases.

Dynamic heterogeneity, another hallmark of glass-like dynamics [35, 36], was calculated using the fourth-order susceptibility [37], $\chi_4(t) = N\left[\langle F_s(k_{\max},t)^2\rangle - \langle F_s(k_{\max},t)\rangle^2\right]$. $\chi_4(t)$ has a broad peak spanning a wide range of times, reflecting the heterogeneous motion of the loci (Fig. S5C). The peak height, χ_4^*, increases till $F \approx 50$ and subsequently decreases (Fig. S5D). When F exceeds 100, χ_4^* decreases precipitously. Our results suggest that there are two transitions: one at $F \approx 50$ where the dynamics slows down and the other, which is a reentrant transition beyond $F = 100$, signaled by an enhancement in the locus mobility. Although the system is finite, these transitions are discernible.

Like the MSD, when $\langle F_s(k_{\max},t)\rangle$ and $\chi_4(t)$ was decomposed into the contributions from A and B loci, we find that the decrease in the dynamics and the enhanced heterogeneity are driven by the active loci (Fig. S6). These observations, including the non-monotonicity in τ_α and β that exhibit a dynamic reentrant behavior, prompted us to examine if the dynamical changes in the A-type loci are accompanied by any structural alterations.

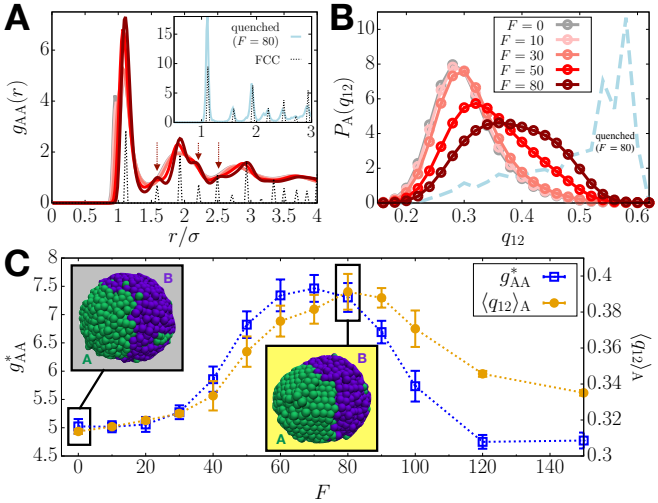

FIG. 3. F-induced crystallization. (A) RDF for A-A locus pairs at different F (solid lines; see the legend in panel B), where $g(r)$ for a FCC crystal is shown with the dotted line (scaled arbitrarily). The inset shows $g_{\text{AA}}(r)$ for the quenched polymer with $F = 80$. (B) Distributions of the BOO parameter, q_{12}, for A loci as a function of F. The dashed line is for the quenched A loci at $F = 80$. (C) Height of the dominant peak in $g_{\text{AA}}(r)$ (blue) and $\langle q_{12}\rangle_{\text{A}}$ (orange) as a function of F. Simulation snapshots for $F = 0$ and $F = 80$ are in the gray- and yellow-background boxes, respectively.

The radial distribution function (RDF) for A-A locus pairs, $g_{\text{AA}}(r)$, with signature of a dense fluid, shows no visible change for $F \lesssim 30$ (Fig. 3A). In contrast, the height of the primary peak, g^*_{AA}, increases sharply beyond $F = 30$ (Fig. 3C). Remarkably, $g_{\text{AA}}(r)$ for $F = 80$ exhibits secondary peaks that are characteristics of a FCC-like solid (arrows, Fig. 3A). Upon further increase in F, these peaks disappear (Fig. S7A) and g^*_{AA} reverts to the level of the passive case (Fig. 3C). In other words,

the active forces, which preserve fluid-like disorder in the A-type loci at low F values, induce a structural transition to FCC-like order in the intermediate range of F values, which is followed by reentrance to a fluid-like behavior at higher F values. In contrast, $g_{\mathrm{BB}}(r)$ exhibits dense fluid-like behavior at all F values (Fig. S7B). We confirm that the FCC lattice is the minimum energy configuration by determining the *inherent structure* for the A loci at $F = 80$ by quenching the active polymer to a low temperature [15, 38, 39] (Fig. 3A, inset). Quenching does not alter the structure of the B loci at $F = 80$ or $g_{\mathrm{AA}}(r)$ at $F = 0$ (Figs. S7C-S7D).

To assess local order, we calculated the bond-orientational order (BOO) parameter for 12-fold rotational symmetry, q_{12} [15, 40, 41]. For a perfect FCC crystal, $q_{12} \approx 0.6$ [42]. The distribution for A loci, $P_{\mathrm{A}}(q_{12})$, is centered around $q_{12} = 0.3$ at $F = 0$ (Fig. 3B), representing a disordered liquid state (gray box, Fig. 3C). As F increases, the distribution shifts towards the right, especially in the $50 \leq F \leq 80$ range. The increase of $\langle q_{12} \rangle_{\mathrm{A}}$ indicates a transition to a FCC-like ordered state that is visible in the simulations (yellow box, Fig. 3C). Although $P_{\mathrm{A}}(q_{12})$ at $F = 80$ is broad due to thermal fluctuations, the inherent structure gives a narrower distribution, peaked near $q_{12} = 0.6$ (dashed line, Fig. 3B). The maximum in $P_{\mathrm{A}}(q_{12})$ shifts to the left for $F > 80$ (Fig. S7E) and $\langle q_{12} \rangle_{\mathrm{A}}$ decreases, suggestive of F-induced reentrant transition. The distribution $P_{\mathrm{B}}(q_{12})$ for the B-type loci is independent of F (Fig. S7F). These results show that FCC-like ordering emerges in $50 \lesssim F \lesssim 100$ range. Outside this range, the RDFs display the characteristics of a dense fluid. The F-dependent bending angle distributions for three consecutive A loci also indicate FCC-like ordering (Fig. S8). The transitions in the A-type loci may be summarized as a fluid $\rightarrow$ FCC $\rightarrow$ fluid, as F changes from 0 to 120.

The predicted transient ordering could be detected by future high resolution imaging experiments. Note that the overall RDF at $F = 80$ does not show FCC peaks (Fig. S9A). Moreover, the correlation function, $C^{\mathrm{A}}_{q_{12}}(t)$ [Eq. (S15)], decays rapidly, at most on the order, ≈ 0.7 s (Fig. S9B), much shorter than the transcription time scale ($\sim$ minute). The ordering preserves the large-scale structure of chromosome (Fig. S10).

The emergence of FCC-like order in the A-type loci could be understood using the effective A-A interaction generated by F. We calculated the *effective* pair potential for an A-A bond, $u_{\mathrm{b}}^{\mathrm{eff}}(r) = u_{\mathrm{b}}^{0}(r) - f_0(r - b_0)$, where $u_{\mathrm{b}}^{0}(r)$ and b_0 are the F-independent bonding potential, and the corresponding equilibrium bond length, respectively. The $f_0(r - b_0)$ term is the work done by the active force to stretch the bond from b_0. Plots of $u_{\mathrm{b}}^{\mathrm{eff}}(r)$ in Fig. 4A show that the effective equilibrium bond length, r_{min}, increases as F increases. This prediction is confirmed by the direct measurement of A-A bond distance from the simulations (Figs. S11A-S11B). Note that $r_{\mathrm{min}}(F = 80) \approx r^*_{\mathrm{LJ}} \approx 1.12\sigma$, where r^*_{LJ} is the distance at the minimum of the LJ potential (Fig. 4B). The F-induced extension of A-A bonds makes r_{min} commensurate with r^*_{LJ}, which is conducive to FCC ordering [43] in the active loci.

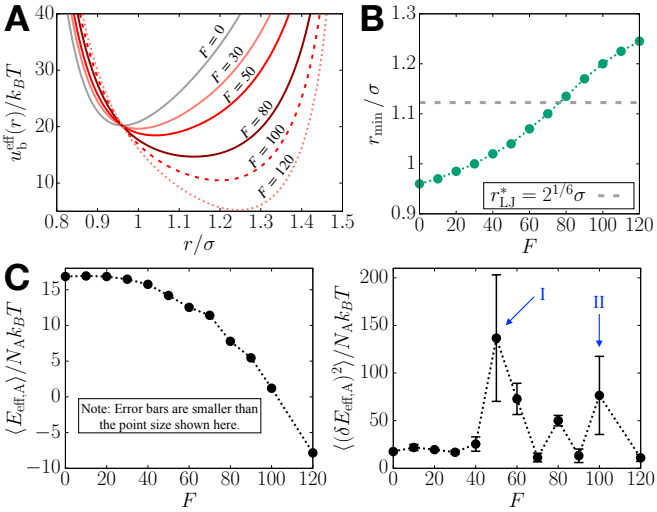

FIG. 4. Effective potential energy accounts for the crystallization of the A-type loci. (A) Effective pair potential of a single A-A bond, $u_{\mathrm{b}}^{\mathrm{eff}}(r)$, as a function of F. (B) Distance at the minimum of $u_{\mathrm{b}}^{\mathrm{eff}}(r)$ as a function of F, where the dashed line indicates r^*_{LJ} (see the main text). (C) Mean of the effective potential energy of A loci (left) and mean fluctuations (right) with respect to F. The arrows indicate the two structural transitions.

We can also describe the ordering behavior using thermodynamic properties based on $u_{\mathrm{b}}^{\mathrm{eff}}(r)$. We calculated the mean and variance of the effective potential energy of the A loci, $E_{\mathrm{eff,A}}$ [15]. Fig. 4C shows that $\langle E_{\mathrm{eff,A}} \rangle$ decreases smoothly as F changes, without pronounced change in the slope, as might be expected for a structural transition [43]. Nevertheless, $\langle (\delta E_{\mathrm{eff,A}})^2 \rangle$ indicates signatures of a transition more dramatically, with peaks at $F = 50$ and $F = 100$ (arrows I and II, Fig. 4C). Thus, both ordering and reentrant fluid behavior coincide with the boundaries of the dynamic transitions noted in Figs. 2B, S5B, and S5D.

To ascertain the robustness of our results, we performed three tests. (1) Simulations for a segment of chromosome 10 with a larger fraction of active loci shows qualitatively similar behavior (Fig. S12). (2) For a copolymer chain whose A/B sequence is random, F does not result in ordering transition (Fig. S13). Thus, F-induced decrease in the motion of the A-type loci, accompanied by transient ordering, occurs only in copolymer chains exhibiting microphase separation between A and B loci—an intrinsic property of interphase chromosomes [44]. (3) We performed simulations using the CCM by removing all the loop anchors (analog of topological constraints [31]). Fig. S14 shows that the F-induced dynam-

ical slowdown and ordering is not significantly affected by the loop anchors.

In the single copolymer chain, which reflects the compact nature of interphase chromosomes [1, 45], transient FCC-like ordering would occur only if the distance between two bonded loci is roughly equal to the distance at which the pair potential between the non-bonded loci is a minimum (for the LJ potential, $r^*_{\rm LJ} = 2^{1/6}\sigma$) [43]. This argument is generic because it only depends on the presence of attractive interactions between non-bonded loci, which is needed to ensure that interphase chromosomes are compact. Application of the active forces increases $r_{\rm min}$, and over a small range of forces $r_{\rm min}$ becomes commensurate with $r^*_{\rm LJ}$ (Fig. 4B). It should be noted that the criterion for FCC-like ordering is *independent* of the interaction parameters characterizing the chromosome, and depends only on the magnitude of the force. If the bonds are rigid, chain segments in the polymer chain, under confinement and active extensile forces, would align exhibiting a nematic order [32]. Thus, the mechanisms of our FCC-like ordering and the nematic order in [32] are qualitatively different. Additional differences between the two models are outlined in [15].

We have discovered a novel mechanism for the dynamical changes upon transcriptional inhibition in mammalian interphase chromosomes, which qualitatively explains the experimental results. Our model has limitations. For instance, explicit effect of transcription factors would bring the theory closer to experiments. Nevertheless, our work elucidates the importance of the effect of active force generated by RNAPII on chromosome. Since the transcription is a stochastic process, with intermittent pauses [46–48], the life time of the ordered phase should be short, and glass-like phase would emerge upon transcription inhibition (Figs. S15-S16). It is likely that the solid-like chromatin observed in the electron microscopy [49] may correspond to the transient order predicted in our study.

We thank Xin Li, Davin Jeong, Kiran Kumari, and Bin Zhang for useful discussions. We thank the National Science Foundation (CHE19-000033) and the Welch Foundation through the Collie-Welch Chair (F-0019) for support.

* Corresponding author: dave.thirumalai@gmail.com

[1] E. Lieberman-Aiden, N. L. van Berkum, L. Williams, M. Imakaev, T. Ragoczy, A. Telling, I. Amit, B. R. Lajoie, P. J. Sabo, M. O. Dorschner, R. Sandstrom, B. Bernstein, M. A. Bender, M. Groudine, A. Gnirke, J. Stamatoyannopoulos, L. A. Mirny, E. S. Lander, and J. Dekker, Science **326**, 289 (2009).

[2] B. Bintu, L. J. Mateo, J.-H. Su, N. A. Sinnott-Armstrong, M. Parker, S. Kinrot, K. Yamaya, A. N. Boettiger, and X. Zhuang, Science **362**, eaau1783 (2018).

[3] E. H. Finn and T. Misteli, Science **365**, eaaw9498 (2019).

[4] I. Bronshtein, E. Kepten, I. Kanter, S. Berezin, M. Lindner, A. B. Redwood, S. Mai, S. Gonzalo, R. Foisner, Y. Shav-Tal, and Y. Garini, Nature Communications **6**, 8044 (2015).

[5] L. Liu, G. Shi, D. Thirumalai, and C. Hyeon, PLOS Computational Biology **14**, e1006617 (2018).

[6] S. S. Ashwin, T. Nozaki, K. Maeshima, and M. Sasai, Proceedings of the National Academy of Sciences of the United States of America **116**, 19939 (2019).

[7] H. A. Shaban, R. Barth, L. Recoules, and K. Bystricky, Genome Biology **21**, 95 (2020).

[8] H. Kang, Y.-G. Yoon, D. Thirumalai, and C. Hyeon, Physical Review Letters **115**, 198102 (2015).

[9] G. Shi, L. Liu, C. Hyeon, and D. Thirumalai, Nature Communications **9**, 3161 (2018).

[10] M. Di Pierro, D. A. Potoyan, P. G. Wolynes, and J. N. Onuchic, Proceedings of the National Academy of Sciences of the United States of America **115**, 7753 (2018).

[11] T. Nozaki, R. Imai, M. Tanbo, R. Nagashima, S. Tamura, and T. Tani, Molecular Cell **67**, 282 (2017).

[12] R. Nagashima, K. Hibino, S. S. Ashwin, M. Babokhov, S. Fujishiro, R. Imai, T. Nozaki, S. Tamura, T. Tani, H. Kimura, M. Shribak, M. T. Kanemaki, M. Sasai, and K. Maeshima, Journal of Cell Biology **218**, 1511 (2019).

[13] B. Gu, T. Swigut, A. Spencley, M. R. Bauer, M. Chung, T. Meyer, and J. Wysocka, Science **359**, 1050 (2018).

[14] M. M. Tortora, H. Salari, and D. Jost, Current Opinion in Genetics and Development **61**, 37 (2020).

[15] See Supplemental Material at [URL] for additional details of the model, simulations, and computations including Figs. S1-S16.

[16] F. Brueckner and P. Cramer, Nature Structural and Molecular Biology **15**, 811 (2008).

[17] O. Bensaude, Transcription **2**, 103 (2011).

[18] H. Yin, M. D. Wang, K. Svoboda, R. Landick, S. M. Block, and J. Gelles, Science **270**, 1653 (1995).

[19] M. D. Wang, M. J. Schnitzer, H. Yin, R. Landick, J. Gelles, and S. M. Block, Science **282**, 902 (1998).

[20] D. Hnisz, K. Shrinivas, R. A. Young, A. K. Chakraborty, and P. A. Sharp, Cell **169**, 13 (2017).

[21] W.-K. Cho, J.-H. Spille, M. Hecht, C. Lee, C. Li, V. Grube, and I. I. Cisse, Science **361**, 412 (2018).

[22] S. Chong, C. Dugast-Darzacq, Z. Liu, P. Dong, G. M. Dailey, C. Cattoglio, A. Heckert, S. Banala, L. Lavis, X. Darzacq, and R. Tjian, Science **361**, eaar2555 (2018).

[23] T. H. S. Hsieh, C. Cattoglio, E. Slobodyanyuk, A. S. Hansen, O. J. Rando, R. Tjian, and X. Darzacq, Molecular Cell **78**, 539 (2020).

[24] Y. Jiang, J. Huang, K. Lun, B. Li, H. Zheng, Y. Li, R. Zhou, W. Duan, C. Wang, Y. Feng, H. Yao, C. Li, and X. Ji, Genome Biology **21**, 158 (2020).

[25] M. L. Huggins, The Journal of Chemical Physics **9**, 440 (1941).

[26] P. J. Flory, The Journal of Chemical Physics **9**, 660 (1941).

[27] S. S. Rao, M. H. Huntley, N. C. Durand, E. K. Stamenova, I. D. Bochkov, J. T. Robinson, A. L. Sanborn, I. Machol, A. D. Omer, E. S. Lander, and E. L. Aiden, Cell **159**, 1665 (2014).

[28] V. Bianco, E. Locatelli, and P. Malgaretti, Physical Review Letters **121**, 217802 (2018).

[29] S. Put, T. Sakaue, and C. Vanderzande, Physical Review E **99**, 032421 (2019).

[30] M. Foglino, E. Locatelli, C. A. Brackley, D. Michieletto, C. N. Likos, and D. Marenduzzo, Soft Matter **15**, 5995 (2019).

[31] J. Smrek, I. Chubak, C. N. Likos, and K. Kremer, Nature Communications **11**, 1 (2020).

[32] D. Saintillan, M. J. Shelley, and A. Zidovska, Proceedings of the National Academy of Sciences of the United States of America **115**, 11442 (2018).

[33] In real units, $\sigma = 0.07\mu$m and $\tau_B = \sigma^2/D_0 = 7 \times 10^{-4}$ s, where D_0 is the diffusion coefficient of a single locus [15].

[34] J. Kim, C. Kim, and B. J. Sung, Physical Review Letters **110**, 047801 (2013).

[35] L. Berthier and G. Biroli, Reviews of Modern Physics **83**, 587 (2011).

[36] T. R. Kirkpatrick and D. Thirumalai, Reviews of Modern Physics **87**, 183 (2015).

[37] T. R. Kirkpatrick and D. Thirumalai, Physical Review A **37**, 4439 (1988).

[38] F. H. Stillinger and T. A. Weber, Science **225**, 983 (1984).

[39] D. Thirumalai, The Journal of Physical Chemistry **93**, 5637 (1989).

[40] P. J. Steinhardt, D. R. Nelson, and M. Ronchetti, Physical Review B **28**, 784 (1983).

[41] P. R. ten Wolde, M. J. Ruiz-Montero, and D. Frenkel, Physical Review Letters **75**, 2714 (1995).

[42] A. K. Omar, K. Klymko, T. Grandpre, and P. L. Geissler, Physical Review Letters **126**, 188002 (2021).

[43] H. W. Cho, G. Shi, T. R. Kirkpatrick, and D. Thirumalai, Physical Review Letters **126**, 137801 (2021).

[44] T. Nagano, Y. Lubling, C. Várnai, C. Dudley, W. Leung, Y. Baran, N. Mendelson Cohen, S. Wingett, P. Fraser, and A. Tanay, Nature **547**, 61 (2017).

[45] L. Manuelidis, Science **250**, 1533 (1990).

[46] R. Landick, Biochemical Society Transactions **34**, 1062 (2006).

[47] X. Darzacq, Y. Shav-Tal, V. De Turris, Y. Brody, S. M. Shenoy, R. D. Phair, and R. H. Singer, Nature Structural and Molecular Biology **14**, 796 (2007).

[48] G. L. Hager, J. G. McNally, and T. Misteli, Molecular Cell **35**, 741 (2009).

[49] H. Strickfaden, T. O. Tolsma, A. Sharma, D. A. Underhill, J. C. Hansen, and M. J. Hendzel, Cell **183**, 1772 (2020).